Published in final edited form as:
Neuroimage. 2013 January 1; 64C: 32–42. doi:10.1016/j.neuroimage.2012.08.071.

Predicting the Location of Human Perirhinal Cortex, Brodmann's area 35, from MRI

Jean C. Augustinack[a,#], **Kristen E. Huber**[a], **Allison A. Stevens**[a], **Michelle Roy**[a], **Matthew P. Frosch**[b], **André J.W. van der Kouwe**[a], **Lawrence L. Wald**[a], **Koen Van Leemput**[a,f], **Ann McKee**[c], **Bruce Fischl**[a,d,e], and **The Alzheimer's Disease Neuroimaging Initiative**[*]

[a]Athinoula A Martinos Center, Dept. of Radiology, MGH, 149 13th Street, Charlestown MA 02129 USA

[b]C.S. Kubik Laboratory for Neuropathology, Pathology Service, MGH, 55 Fruit St., Boston MA 02115 USA

[c]Department of Pathology, Boston University School of Medicine, Bedford Veterans Administration Medical Center, MA 01730 USA

[d]MIT Computer Science and AI Lab, Cambridge MA 02139 USA

[e]MIT Division of Health Sciences and Technology, Cambridge MA 02139 USA

[f]Department of Informatics and Mathematical Modeling, Technical University of Denmark, Copenhagen, Denmark

Abstract

The perirhinal cortex (Brodmann's area 35) is a multimodal area that is important for normal memory function. Specifically, perirhinal cortex is involved in detection of novel objects and manifests neurofibrillary tangles in Alzheimer's disease very early in disease progression. We scanned *ex vivo* brain hemispheres at standard resolution (1 mm × 1 mm × 1 mm) to construct pial/white matter surfaces in FreeSurfer and scanned again at high resolution (120 μm × 120 μm × 120 μm) to determine cortical architectural boundaries. After labeling perirhinal area 35 in the high resolution images, we mapped the high resolution labels to the surface models to localize area 35 in fourteen cases. We validated the area boundaries determined using histological Nissl staining. To test the accuracy of the probabilistic mapping, we measured the Hausdorff distance between the predicted and true labels and found that the median Hausdorff distance was 4.0 mm for left hemispheres (n = 7) and 3.2 mm for right hemispheres (n = 7) across subjects. To show the utility of perirhinal localization, we mapped our labels to a subset of the Alzheimer's Disease Neuroimaging Initiative dataset and found decreased cortical thickness measures in mild cognitive impairment and Alzheimer's disease compared to controls in the predicted perirhinal area 35. Our *ex vivo* probabilistic mapping of perirhinal cortex provides histologically validated, automated

[#]Author to whom correspondence should be addressed: Jean Augustinack Athinoula A Martinos Center Massachusetts Gen. Hosp/ Harvard Med. School Bldg. 149, 13th St. Charlestown, MA 02129 tel: 001 617 724-0429 fax: 001 617 726-7422 jean@nmr.mgh.harvard.edu.

[*]Data used in preparation of this article were obtained from the Alzheimer's Disease Neuroimaging Initiative (ADNI) database (adni.loni.ucla.edu). As such, the investigators within the ADNI contributed to the design and implementation of ADNI and/or provided data but did not participate in analysis or writing of this report. A complete listing of ADNI investigators can be found at: http://adni.loni.ucla.edu/wp-content/uploads/how_to_apply/ADNI_Acknowledgement_List.pdf

and accurate labeling of architectonic regions in the medial temporal lobe, and facilitates the analysis of atrophic changes in a large dataset for earlier detection and diagnosis.

Keywords

morphometry; mesocortex; Alzheimer's disease; localization

INTRODUCTION

Perirhinal cortex (Brodmann's area 35) is a multimodal cortical area that is located in the medial temporal lobe (MTL). A multimodal area receives input from more than one cortical association area and it is a region where information from different modalities converge (Van Hoesen 1975, Jones and Powell 1970). Perirhinal cortex is situated between entorhinal cortex (Brodmann's area 28 and perirhinal's medial neighbor) and ectorhinal cortex (Brodmann's area 36 and perirhinal's lateral neighbor) in the mediolateral plane. The ectorhinal cortex (area 36) constitutes perirhinal's anterior and lateral neighbor while the posterior parahippocampal cortex lies posterior to perirhinal cortex.

Brodmann described perirhinal cortex as a “transition between archipallium and neopallium” (Brodmann, 1909; Brodmann and Garey, 1994). Since then, perirhinal cortex has undergone several name modifications. Braak and Braak coined the term `transentorhinal' and succinctly described the mediolateral boundaries, but this description lacked the anterior-posterior entirety of the area (Braak and Braak, 1985). Perirhinal area 35 and transentorhinal are somewhat synonymous terms. To further complicate the situation for area 35, several investigators have lumped area 35 (perirhinal) and area 36 (ectorhinal) together and referred to it as perirhinal cortex (Suzuki and Amaral, 1994a, b), dropping the ectorhinal designation entirely and creating a very large area. Nonetheless, extensive rostrocaudal analyses with several histological stains have yielded the boundaries of perirhinal cortex in the human brain, albeit including isocortical area 36 in the definition (Ding and Van Hoesen, 2010). To make matters even more confusing, perirhinal (area 35) and entorhinal (area 28) have also been grouped together and referred to as rhinal cortex (Meunier et al., 1996; Murray and Mishkin, 1986). As a result, perirhinal cortex has three names and three different meanings in the current literature. Given that perirhinal cortex lies in the depths of two sulci (the rhinal sulcus anteriorly and the collateral sulcus anteriorly and posteriorly), and that perirhinal cortex has several names and designations, its location has been confounded with that of its neighbors. This complicated and convoluted scientific backdrop with respect to perirhinal is unfortunate, because imaging, cognitive, and behavioral neuroscientists rely on accurate neuroanatomical localization. When loose definitions occur anatomically, it is difficult to interpret functional findings and controversies can develop that are more semantic than substantive.

Regarding function, perirhinal cortex plays a significant role in memory as has been demonstrated by several lines of evidence. Perirhinal cortex detects novel objects and denotes familiarity both in non-human primate studies and functional MRI (Buckley and Gaffan, 1998; Meunier et al., 1993; Meunier et al., 1996; Murray et al., 2005; Murray and Mishkin, 1986; Suzuki et al., 1993; Zola-Morgan et al., 1989). Perirhinal cortex receives inputs from a plethora of diverse cortices and its strongest output projects to entorhinal cortex, its medial neighbor, (Suzuki and Amaral, 1994a, b; Van Hoesen and Pandya, 1975a), which in turn projects to the hippocampus (Van Hoesen 1975b). Undeniably, all of these structures, entorhinal, perirhinal and hippocampus are well known for their role in memory (Brown and Aggleton, 2001; Murray et al., 2005). In fact, when the memory circuit fails as it does in Alzheimer's disease, the medial temporal lobe reveals a burden of neurofibrillary

tangles and beta-amyloid plaques (Arnold et al., 1991a; Braak and Braak, 1991). Moreover, perirhinal cortex manifests neurofibrillary tangles in normal aging and Alzheimer's disease (AD) at its earliest pathological stages in the MTL (Braak and Braak, 1985; Knopman et al., 2003; Kordower et al., 2001; Solodkin and Van Hoesen, 1996; Van Hoesen et al., 2000). As the disease progresses, neurofibrillary tangles and amyloid plaques dominate the entire cerebral cortical landscape, and replace healthy neurons with dysfunctional tangled ones and extracellular deposits (Arnold et al., 1991a; Braak and Braak, 1991). This massive neuronal cell death throughout MTL (and beyond in later stages) causes significant atrophy that has been detected with *in vivo* MRI. Several groups have demonstrated that entorhinal and perirhinal show volumetric changes between normal aging and mild Alzheimer's disease (De Toledo-Morrell et al., 2000; Jack et al., 1997; Kaye et al., 1997; Killiany et al., 2000; Killiany et al., 2002; Xu et al., 2000) and the mesocortices represent the best indicators, and even more so, the predictors of converting to AD.

Currently, standard clinical MRI scans are acquired with voxels that are approximately 1–2 mm and are thus unable to resolve cortical architecture detail. A recent field has emerged called `*ex vivo* imaging' where an autopsy brain is scanned allowing for the acquisition of ultra-high resolution images due to a number of factors that increase image SNR dramatically (e.g. no sample motion, optimal coil loading, exceptionally long scan sessions, reduced distance of the coils from the sample). Generating probabilistic maps based on *ex vivo* imaging has become a reliable method to predict location and cortical boundaries because it can be validated with histological ground truth (Fischl et al., 2009). *Ex vivo* probability maps have improved upon a global volumetric registration such as the Talairach atlas or relying on cortical folding patterns in an *ad hoc* manner, which can be problematic in higher order associative areas where the sulcal pattern is quite variable.

Our goal was to define perirhinal cortex (area 35) in *ex vivo* MRI, validate the MRI-based labeling with Nissl staining, and build a probabilistic atlas for this area in FreeSurfer (http://surfer.nmr.mgh.harvard.edu/fswiki). In this study, we utilized probabilistic mapping based on high resolution *ex vivo* imaging to predict the location of perirhinal cortex in the human brain, validated them with histological assays and applied our mesocortical (i.e. entorhinal and perirhinal) labels to the Alzheimer's Disease Neuroimaging Initiative (ADNI) dataset to assess cortical thickness in these vulnerable areas in the MTL in aging, mild cognitive impairment and Alzheimer's disease.

MATERIALS AND METHODS

Ex vivo samples

We collected 14 autopsied brain hemispheres from the Massachusetts General Hospital Autopsy Service (Massachusetts General Hospital, Boston MA) and the Framingham Heart Study and Boston University Alzheimer's Disease Center (Veterans Administration Medical Center, Bedford, VA). Each case was pathologically screened for overt neurological diagnoses such as strokes or significant atrophy and none was reported. Hemisphere laterality was evenly divided in our *ex vivo* sample set with seven left hemispheres and seven right hemispheres. The mean age was 66.9 years and standard deviation was 9.8 years. We procured 8 male and 2 female cases while in the remaining four cases gender information was unavailable. The postmortem interval was restricted to be less than 25 hours and our sample set had a mean PMI of 20.6 hours and standard deviation of 5.6 hours. Before scanning, each hemisphere was visually inspected for abnormalities and none were observed. These *ex vivo* cases were used for labeling and probabilistic mapping, as described in the following sections.

Radio frequency coils

We acquired images using two custom-made coils (Martinos Center for Biomedical Imaging, Charlestown MA) depending on whether we imaged perirhinal cortex within a hemisphere or excised the MTL to create a block. For the hemispheres, we utilized a 4-channel phased array coil that consisted of 4 loop coil elements that were 5 cm in diameter and overlapped 1.5 cm with neighboring elements. The combined length of the 4 intertwining coils was approximately 16 cm. For the MTL blocks we utilized a 4-turn solenoid with 28.5 mm inner diameter and 44 mm in length. For scanning, the hemisphere samples were packed in a plastic bag and vacuum sealed while the solenoid samples were packed in a plastic test tube (i.e. Falcon tube) and inserted into the solenoid holder.

Ex vivo imaging and acquisition

We used a fast low angle shot (FLASH) sequence on a 7.0 T human scanner from Siemens (Siemens Healthcare, Erlangen, Germany). Our standard resolution for the high resolution *ex vivo* samples was 120 μm isotropic for all cases except two cases where the resolution was 100 μm isotropic. We determined that a resolution of 120 μm in lieu of 100 μm still adequately revealed the relevant histoarchitectural (i.e. laminar) features with shortened scan time and increased SNR. We have optimized scan parameters in previous studies (Augustinack et al., 2005; Fischl et al., 2009) and found that a flip angle of 20° resulted in the best contrast to noise ratio per unit time. Furthermore, we set TR = 40 ms and TE = 20 ms and found that an echo time set at half the repetition time for *ex vivo* imaging produced consistent contrast quality and increased SNR when minimizing the bandwidth. It should be noted though that even though parameters were consistently controlled at standard settings, brain samples can yield various contrasts visually. In addition to the high resolution *ex vivo* images, we acquired MRI volumes of the entire brain hemispheres at lower resolution, 1.0 mm × 1.0 mm × 1.0 mm so that we could create surface models and transform the label from the high resolution data to the lower resolution images for the purpose of creating the probabilistic maps for perirhinal cortex based on spherical warping (Fischl et al., 1999a).

Neuroanatomical Labeling

In previous studies (Fischl et al., 2009), we established a labeling protocol based on architectonic features observed in *ex vivo* MRI. We followed the topographical anatomy and cortical architecture described in previous reports (Braak and Braak, 1985; Ding and Van Hoesen, 2010; Van Hoesen et al., 2000). In this report, we labeled perirhinal cortex, Brodmann's area 35, based on vertical modular columns in area 35a and an oblique wedge that is located between layers III–VI in area 35b. Lighter signal intensity was observed in neighboring ectorhinal (Brodmann area 36) along all cortical layers unlike the more superficial signal increase observed in perirhinal area 35. The perirhinal label described in this report will be publically released in FreeSurfer.

Terminology

Perirhinal cortex is a bipartite cortex composed of periallocortex for area 35a and proisocortex for area 35b (Sanides, 1969, 1970; Van Hoesen and Pandya, 1975a). This bipartite observation was first noticed by Sanides in early 1970's (Van Hoesen and Pandya, 1975a) and carried forth by Van Hoesen (Van Hoesen et al., 2000) and colleagues (Ding and Van Hoesen, 2010). Mesocortex is a generic term that includes both periallocortex and proisocortex and that indicates the paralimbic belt of the cerebral cortex (Mesulam and Mufson, 1985; Pandya and Yeterian, 1985). This paralimbic or mesocortical belt of cortex intervenes between three-layered (i.e. paleocortex or allocortex) cortex and six-layered (i.e. neocortex, isocortex) cortex.

Registration

We used Register (MNI toolkit, Montreal, Canada, http://www.bic.mni.mcgill.ca) for all registrations that were performed in this study. We registered the FreeSurfer reconstructions to the higher resolution images that contained anatomical labels based on cortical architectural fields observed at ~120 μm. We used a 12-parameter affine registration in Register and manually set fiducial tags on corresponding points on the low and high resolution images, and used the correspondences to create a transform. This protocol was repeated for each case. After visual inspection, multiple registrations were performed using Register to refine and obtain the best possible registration. In *ex vivo* imaging, we, of course, have no head landmarks to ascertain customary coronal, axial and sagittal planes; thus, after MRI acquisition we rotated cases to a standard orientation and aligned to our histological coronal plane. For the labeling, we occasionally observed sites that required manual editing of the high resolution labels (just editing a voxel or two voxels to account for errors sampling onto the surface) and these small edits did not significantly change the overall label. Given that perirhinal primarily resides along sulci, perirhinal labels were prone to "leaking" into abutting gray matter in the sulcus due to small mis-registration between the high resolution and low resolution volumes, necessitating a small amount of manual editing.

Participants and ADNI image acquisition

Data used in preparation of this article were obtained from the Alzheimer's Disease Neuroimaging Initiative (ADNI) database (www.loni.ucla.edu/ADNI) (Petersen et al., 2010). The ADNI was launched in 2003 by the National Institute on Aging, the National Institute of Biomedical Imaging and Bioengineering, the Food and Drug Administration, private pharmaceutical companies, and nonprofit organizations, as a $60-million, 5-year public-private partnership. The primary goal of ADNI is to test whether imaging measures, biological markers, and clinical and neuropsychological assessment can be combined to measure the progression of MCI and early AD. Detailed diagnostic, inclusion, and exclusion criteria are described on the ADNI Web site (http://www.adni-info.org/). Each participant gave written informed consent in accordance with institutional Human Subjects Research Committee guidelines.

MRI scans were collected on a 1.5 T scanner using a standardized magnetization-prepared rapid gradient echo protocol (Mugler and Brookeman, 1991): sagittal plane, repetition time/ echo time/inversion time, 2,400/3/1,000 ms, flip angle 8°, 24 cm field of view, 192 × 192 in-plane matrix, 1.2 mm slice thickness (Jack et al., 2008).

We selected 740 subjects from the ADNI database that also produced good reconstructions from the FreeSurfer stream (FreeSurfer, Charlestown MA http://surfer.nmr.mgh.harvard.edu) (Dale et al., 1999; Fischl et al., 2001; Fischl et al., 1999a; Fischl et al., 1999b; Segonne et al., 2004). All subjects were analyzed at baseline. The gender split included 436 males and 304 females. The diagnoses were normal controls (NC, n=215), mild cognitive impairments (MCI, n=358) and Alzheimer's disease (AD, n=167). The mean age for the control group was 75.9 years with standard deviation 5.5 years while the mild cognitive impairment group had a mean age of 75.0 years with standard deviation 7.1 years and Alzheimer's group presented a mean age of 75.5 years with standard deviation 7.7 years. Thus, the three groups were age matched with a mean of approximately 75 years old. We used the FreeSurfer surfaces from these ADNI cases and our perirhinal and entorhinal labels to evaluate the cortical thickness in perirhinal and entorhinal cortices, respectively.

Statistics

For the cortical thickness analyses, we used a t-test in Matlab (Mathworks, Natick MA) to test the significance between diagnoses (normal, mild cognitive impairment and Alzheimer's subjects). For each label, the vertices were ordered from most probable least probable), then thresholded so that the surface area of each predicted entorhinal cortex or perirhinal cortex label matched the average surface area of the *ex vivo* labels.

RESULTS

Boundaries of perirhinal cortex

Several cortical architectural features defined perirhinal cortex in MRI FLASH images. First, modularity was revealed by alternating light and dark intensity that was observed in perirhinal area 35a. Second, dark signal was observed in the superficial layers in area 35a and 35b, but this dark signal was only observed in infragranular layers in area 35a. Thus, the dark signal formed an oblique wedge throughout the anterior-posterior extent of perirhinal cortex. The superficial layers of perirhinal area 35b showed a lighter intensity in FLASH images compared to its inferior layers (i.e. layers IV (dysgranular), V, VI). The modularity and the wedge segment were consistently observed along the anterior-posterior axis and illustrated in one sample case (Fig. 1). White arrowheads show medial and lateral borders of perirhinal cortex. Anteriorly at the level of the primary olfactory cortex, we have demonstrated our first MRI slice with perirhinal cortex. The vertical columns and disparity in contrast between supragranular and infragranular layers were observed on the lateral parahippocampal gyrus (at this particular anterior-posterior level) and also on the medial bank of the collateral sulcus (Fig. 1A). At the rostral boundary as well as the caudal boundary (shown later), perirhinal occupied part of the parahippocampal gyrus surface so that it came into view on the exposed gyrus from the depths of the sulcal topography. Moving posteriorly, perirhinal cortex is positioned more laterally and in the next illustrated MRI slice, we observed perirhinal cortex in the medial bank of the collateral sulcus and it no longer resided on the parahippocampal surface (Fig. 1B). The complex sulcal pattern of the human brain routinely creates a unique topography for perirhinal cortex for each individual. The lighter signal in superficial layers in area 35b and the subsequent wedge was a telltale sign of Brodmann's area 35b in *ex vivo* imaging. Perirhinal cortex continued in this location for several slices (Fig. 1C–1F) and the bulk of perirhinal cortex resided on this medial bank. If the depth of collateral sulcus was shallow, we observed perirhinal cortex on the collateral sulcus medially but also found it overflowed slightly onto the lateral bank as well (Fig. 1G–I). In most of our cases, perirhinal cortex obeyed the medial bank of the collateral sulcus and the fundus of the collateral sulcus marked the lateral boundary at this mid-rostrocaudal level. Nonetheless, when the sulcus was shallow or in the posterior perirhinal as the collateral sulcus ended, it was common for the perirhinal cortex to splay past the collateral fundus and slightly occupy the top of the lateral bank (Fig. 1J–K). The last panel (Fig. 1L) shows the perirhinal cortex positioned on the surface on the parahippocampal gyrus, posterior to where entorhinal cortex ended. Posteriorly, perirhinal ended approximately at the level of the lateral geniculate nucleus of the thalamus and ended in most cases as the collateral sulcus ended (but slightly more posterior about 1 mm, less than 10 MRI slices at 100 μm^3). Thus, the landmarks that defined the mediolateral boundaries changed slightly throughout the anterior-posterior extent of parahippocampal gyrus. Perirhinal cortex extended beyond entorhinal cortex and encompassed entorhinal cortex on all entorhinal sides, anteriorly, posteriorly and medially and was on the exposed parahippocampal surface at the anterior and posterior limits.

Histological-MRI Validation of Perirhinal Cortex

We identified perirhinal cortex, Brodmann's areas area 35, in high resolution *ex vivo* MRI and in Nissl stained histological sections. The Nissl stained sections were used to guide the detection of cortical architectural *ex vivo* MRI features. The high resolution *ex vivo* MRI showed modularity in superficial perirhinal cortex and layers II and III were organized into vertical columns (Fig. 2A). The vertical columns were evenly spaced and were present in area 35a. The medial border of perirhinal cortex is adjacent to entorhinal cortex and resides just inside the parahippocampal gyrus immediately medial to the collateral sulcus (Fig. 2). In this case, the border is not exactly on the bend of the parahippocampal crown but a few millimeters further inside the sulcus (within inset c in Fig. 2B). The depth of perirhinal columns depended on the depth of the collateral sulcus. The example in Figure 2 illustrates a fairly shallow collateral sulcus therefore the perirhinal columns exhibited relatively short columns (Fig. 2C). Nevertheless, the vertical columns displayed in close proximity to each other were visually distinct. Recognizably, the perirhinal columns showed greater depth than the entorhinal islands that only encompass layer II. Both the perirhinal columns and entorhinal islands showed as bright intensities on *ex vivo* FLASH images (Fig. 2A). In this image, the brightness and contrast were optimized for perirhinal cortex. Entorhinal cortex appears somewhat dim. Perirhinal area 35b lies more dorsally than perirhinal area 35a and was located closer to the collateral sulcus fundus (Fig. 2A, 2B). In its superficial layers, area 35b contains a wedge that has been described histologically (Braak and Braak, 1985) and we observed this oblique slant in *ex vivo* MRI and found it an extremely reliable feature to identify perirhinal cortex. The lateral border of perirhinal cortex is adjacent to ectorhinal cortex (Brodmann's area 36) and the boundary typically rests at the fundus of the collateral sulcus. In area 35b, the organization of the columns was not observed in superficial layers, yet we observed the deep layers of area 35b demarcated by a dark region in *ex vivo* MRI as well as histology (Fig. 2D). The oblique slant of this region was larger (vertically in the pia-white matter plane) in the more medial portion of 35b and narrowed laterally toward the fundus for area 35b. The area 35b - area 36 border showed differences in signal properties, with no oblique contrast in superficial layers but bright signal intensity for these layers in ectorhinal area 36.

To validate what we observed in MRI, we demonstrated the cytoarchitectural organization in Nissl sections (Fig. 2B) and illustrated area 35a and area 35b on the medial bank of the collateral sulcus on this particular section. In this MTL block, many areas occupy this small region and in addition to the mesocortices, hippocampus and subicular cortices show distinct cortical cellular organization. High magnification photomicrographs illustrate the laminar organization in perirhinal cortex (Fig. 2C and 2D). Perirhinal area 35a and area 35b have a vastly different architecture as illustrated in Fig 2C and 2D. Black arrows show the perirhinal columns while a single black arrowhead shows the lateral-most entorhinal island. The beginning of the wedge was demarcated with gray dotted lines in Fig 2C for perirhinal area 35a and continued in Figure 2D for perirhinal area 35b while the asterisk in Fig. 2D denotes layer V in area 35b.

Perirhinal surface models

Two sets of MRI data were acquired, consisting of 1 mm^3 *ex vivo* data collected at 1.5 T and 100 μm isotropic *ex vivo* data collected at 7.0 T. The 1 mm^3 data was used to create a surface model for each individual case while the 100 μm data was used to delineate cortical lamina for perirhinal cortex and demarcate perirhinal boundaries. Each case was manually labeled for perirhinal cortex based on laminar observations in the high resolution *ex vivo* MRI. Once the entire extent of perirhinal cortex was labeled, we manually registered the labeled high resolution data to the low resolution images and used a rigid transformation to move labels from high resolution to low resolution images. From that transformation, we

generated individual maps for left and right hemispheres (Fig. 3). The white label represents perirhinal cortex (Brodmann's area 35) on the individual subject inflated surface maps.

To visualize the distance between labels, we used a common spherical coordinate system (Fischl et al., 1999a; Fischl et al., 1999b) and an existing template - fsaverage (FreeSurfer average) - to display a multiple subject spatial probability map in FreeSurfer. Each vertex on the average map was registered with vertices from each subject to determine colocalization of the perirhinal labels. Color labels (red and yellow) represent overlap within perirhinal labels whereas gray surface contains no perirhinal label (Fig. 4). Yellow represents 100% overlap, while gray represents 0% overlap of vertices. Dark and light gray correspond to cortical sulci and gyri, respectively. These probabilistic maps show the location of perirhinal cortex in the anterior parahippocampal gyrus and more specifically that perirhinal cortex is located in medial bank of collateral sulcus but also is positioned on the parahippocampal surface at the anterior and posterior ends (Fig. 4). The probabilistic average for perirhinal area 35 is shown on an inflated fsaverage template.

Measurement and accuracy of surface models

To quantify the variability of perirhinal cortex in our cases, we applied a modified symmetric Hausdorff distance (HD). The HD is a set theoretic measure that allows one to measure the “distance” between two point clouds. Typically the HD is defined as the maximum overall minimum distances between each point in one set to all the points in the other. This can be symmetrized by averaging the HD for the two directions (i.e. from set A to set B and from B to A). In addition, we have found the median to be a more stable measure than the maximum, so it is what we report here. The median HD was 4.0 mm for left hemispheres (n = 7) and 3.2 mm for right hemispheres (n = 7) (Fig. 5) across subjects (that is, transforming each subject's perirhinal label through the spherical mapping, to every other subject, then computing the HD between the manual and the mapped labels). The left hemisphere showed slightly more variability than the right hemisphere.

Application of perirhinal surface models

To demonstrate the utility of the probabilistic mapping, we applied our probabilistic localization to a subset of ADNI participants. We limited the ADNI image volumes to datasets that contained good quality reconstructions and accurate spherical registration. We examined the cortical thickness in perirhinal cortex (defined as area 35) and in entorhinal cortex (defined as area 28) in the selected ADNI dataset of normal controls, (NC, n = 215, mean age = 75.9 years ± 5.5), mild cognitive impairment (MCI, n=358, mean age = 75.0 years ± 7.1) and Alzheimer's disease (AD, n = 167, mean age = 75.5 years ± 7.7). The cortical thickness was larger for the control group in both predicted locations of perirhinal and entorhinal cortex. The perirhinal cortex (black bars, Fig. 6) was slightly smaller than entorhinal cortical thickness (gray bars, Fig. 6) and with each diagnostic increment of disease (NC > MCI > AD). Thus, the cortical thickness was smaller in MCI and AD compared to normal controls (Fig. 6). Error bars stand for standard error of the mean for each group. Perirhinal thickness in normal controls was approximately 3.15 mm and decreased with MCI diagnosis to 2.8 mm and to 2.5 mm in AD in the left hemispheres. The same pattern was observed in the right hemisphere where controls showed a cortical thickness of 3.15 mm, MCI patients showed 2.8 mm and AD showed 2.5 mm. The differences were highly statistically different among each diagnostic group ($p < 1.0^{-9}$ and $t < 1.0^{-15}$). A similar progressive degenerative cortical thickness pattern was observed in entorhinal cortex on the right and left but the entorhinal cortex thickness was slightly larger by approximately 0.2 mm – 0.4 mm. These results suggest an accurate means to evaluate atrophy in MTL structures.

DISCUSSION

In this report, we identified the location of perirhinal cortex (Brodmann's area 35) using high resolution *ex vivo* MRI, validated perirhinal cortex with histological analysis and applied surface based registration to our labeled perirhinal cortices to quantify the variability between subjects. We then utilized the labels to predict perirhinal cortex location in ADNI *in vivo* subjects and applied it to determine cortical thickness in controls, mild cognitive impairment and AD patients in Brodmann's area 35.

Perirhinal cortex (area 35) has similarities and differences from its neighboring regions, entorhinal cortex (area 28) and isocortical area 36. Modularity or a clustering of neurons in the superficial layers is typically observed in entorhinal area 28 and perirhinal area 35a and has been referred to as entorhinal islands and perirhinal columns, respectively. The modularity in perirhinal cortex includes not only layer II but also layer III, so that layers II–III make up the vertical column (Braak and Braak, 1985; Solodkin and Van Hoesen, 1996; Van Hoesen et al., 2000; Van Hoesen and Solodkin, 1993). This modularity observed in area 28 and area 35a is a classic attribute of the periallocortex tissue type. Perirhinal area 35a is agranular cortex which means that layer IV is absent. More specifically, a placeholder layer occurs spatially in layer IV but with no cells present. Perirhinal area 35b is proisocortex with a dysgranular layer IV, which means it has a few cells in layer IV but not completely organized yet. The organization of layer IV is one of the major differences between area 35 and area 36 (Ding and Van Hoesen, 2010; Ding et al., 2009; Insausti et al., 1998; Sanides, 1969). While area 35 is agranular and dysgranular (35a and 35b, respectively), area 36 contains a compact and granular layer IV. Layer V has medium sized pyramidal neurons in perirhinal area 35a and 35b, but layer V in 35b is more organized and uniform compared to area 35a. Layer V in area 35b starts to resemble the internal pyramidal layer of isocortical areas but is not as thick, typically only one or two neurons. Layer V and VI are positioned closely together in entorhinal, perirhinal and ectorhinal cortices. Thus, area 35 is periallocortex and proisocortex with agranular and dysgranular lamination patterns, respectively, while area 36 is isocortex because it has a distinct and granular layer IV (Gloor, 1997; Sanides, 1969; Stephan, 1975). Area 36 contains all the components that quintessentially define isocortex proper – thick layer I, granular layer IV, pyramidal neurons in layers III and V (Ding and Van Hoesen, 2010; Ding et al., 2009; Gloor, 1997; Insausti et al., 1998; Sanides, 1969; Stephan, 1975; Suzuki and Amaral, 2003a, b). Area 35 and area 36 also reveal distinct and different staining in immunocytochemical labeling in calcium binding proteins (calbindin-Dk28, parvalbumin), non-phosphorylated neurofilament protein (SMI-32), Wisteria floribunda agglutinin, and phosphorylated tau (AT8) (Ding and Van Hoesen, 2010).

As mentioned in the introduction, a confusing nomenclature has burdened perirhinal cortex and contributed to its mis-localization. Brodmann described perirhinal cortex as a “transitional cortex between archipallium and neopallium” (Brodmann, 1909; Brodmann and Garey, 1994) and while this may be, it saddled perirhinal cortex with a poor connotation. Braak continued this by coining the term `transentorhinal' cortex for perirhinal area 35 (Braak and Braak, 1985) and others have followed (Taylor and Probst, 2008). Brodmann also described perirhinal cortex as “[consisting] of a narrow strip-like zone limited to the rhinal sulcus and its immediate surroundings that follows this sulcus along its whole length, extending a little beyond it caudally” (Brodmann, 1909; Brodmann and Garey, 1994). Brodmann underestimated the size of perirhinal area 35. In fact, perirhinal cortex (area 35) may be slightly larger than entorhinal cortex (area 28) because perirhinal surrounds entorhinal on three sides (medially, anteriorly, and posteriorly) but this size depends on the sulcal depth. The nomenclature has been further complicated since several studies have grouped area 35 (perirhinal) and area 36 (ectorhinal) together (Ding and Van Hoesen, 2010;

Insausti et al., 1998; Suzuki and Amaral, 1994a, b). The grouping of area 35 and area 36 was an unfortunate event but likely occurred due to non-human primate studies where it was difficult to target only one Brodmann area, or there was similar connectivity (e.g. Suzuki and Amaral argued that areas 35 and 36 produced similar connectivity in the macaque but included area TE in their explanation) (Suzuki and Amaral, 1994a), differences in evolutionary animal anatomy, or misidentification due to confusing sulcal patterns. It may even be that the term ectorhinal was dismissed because it is too similar in spelling to entorhinal with just one letter difference between them. It is important to note that areas 36 and 20 (visual association areas) correspond approximately to visually dominant areas (TE of von Economo) (von Economo and Koskinas, 1925), which are isocortical areas while perirhinal cortex (area 35) is a periallocortical-proisocortical multimodal area. Several additional studies have categorized area 28 and area 35 together as rhinal cortex. The mesocortices may have been grouped for similar reasons as described above, or due to an inclination to keep continuity with the rodent brain. Thus, categorically, perirhinal cortex has been merged with entorhinal cortex medially (i.e. rhinal cortex) (Meunier et al., 1993; Murray and Mishkin, 1986) or with ectorhinal cortex (area 36) laterally (Ding and Van Hoesen, 2010; Insausti et al., 1998; Suzuki and Amaral, 1994b), but also alone (Solodkin and Van Hoesen, 1996; Van Hoesen et al., 2000; Van Hoesen and Pandya, 1975b; Van Hoesen and Solodkin, 1993).

Teasing out area 35 analyses from previous studies that have merged perirhinal area 35 with other above mentioned areas (entorhinal or area 36), our MRI detection of perirhinal cortex agrees with (Ding and Van Hoesen, 2010) and (Insausti et al., 1998) for the anterior-posterior extent for area 35 analyses only in that it extends from temporal incisura anteriorly to slightly past the level of the lateral geniculate nucleus of the thalamus posteriorly. Moreover, we determined that Sanides' anatomical description of 35a and 35b was the most consistent with our *ex vivo* MRI and corresponding Nissl analysis. Our results also agree with Braak (Braak and Braak, 1985) and Van Hoesen (Van Hoesen et al., 2000) regarding the medial-lateral boundaries among areas 28, 35 and 36. Due to the location of perirhinal cortex spanning two gyri, multiple names have emerged. Insausti described 35v and 35o where area 35 ventral roughly corresponds to anterior area 35 at the temporal incisura (Insausti et al., 1998) and Insausti's 35o represents area 35 oblique and corresponds to the bulk of area 35, along the medial bank of the collateral sulcus, (i.e. Braak's transentorhinal) (Braak and Braak, 1985; Ding and Van Hoesen, 2010; Van Hoesen and Solodkin, 1993). These studies also noted the columnar regions (area 35a) and oblique wedge in lateral perirhinal cortex (area 35b). Our *ex vivo* MRI images revealed this pattern and displayed the oblique pattern anteriorly, aligned on the medial bank of the collateral sulcus at the level of the amygdala, and continuing posteriorly until the sulcus ends.

It could be postulated whether the architecture of perirhinal area 35 represents a distinct pattern, or is a continuum between entorhinal and ectorhinal (area 36) cortices. Based on the fact that perirhinal's architecture is consistent from brain to brain, our data and others' support a specific pattern for perirhinal cortex, although there may be some truth to the continuum perspective as well. It could be a continuum because it contains features that resemble entorhinal cortex medially and temporal isocortex (area 36) laterally. The former description - a specific pattern - is preferred due to the distinct cortical architecture and the considerable size of area 35. Our probabilistic map of perirhinal cortex rivals the size of our probabilistic map for entorhinal cortex (Fischl et al., 2009) and this agrees with others that have shown the extensive size of perirhinal cortex (Braak, 1980; Ding and Van Hoesen, 2010; Insausti et al., 1998). Given that the mesocortical (i.e. paralimbic) belt intervenes between allocortex and isocortex, transitional cortices have been observed with retrosplenial cortex as well that show a different pattern (Braak, 1980), which argues for the condition that perirhinal cortex exhibits a specific pattern of cortical architecture. We recommend

referring to area 36 as `isocortical area 36' and only using the term perirhinal cortex to refer to area 35 in future publications.

Several studies have investigated the relationship between myelin content and *ex vivo* contrast (Augustinack et al., 2010; Bock et al., 2009; Eickhoff et al., 2005; Geyer et al., 2011). In *ex vivo* MRI of fixed tissue, a variety of contrasts have been reported that correlate with myelin content, T2* (Fukunaga et al., 2010), T2 (Augustinack et al., 2010; Eickhoff et al., 2005) as well as T1 (Bock et al., 2009; Geyer et al., 2011) and phase (susceptibility weighted) (Duyn et al., 2007; Langkammer et al., 2012). The medial temporal lobe and in particular entorhinal and perirhinal cortices are not generally heavily myelinated with the exception of the alveus and the molecular layer of the presubiculum (the superficial presubicular pathway) (Rosene and Van Hoesen, 1987). Nonetheless, myeloarchitecture in perirhinal cortex provides excellent *ex vivo* contrast. Braak described and illustrated the cyto-, pigmento- (relating to lipofuscin granules) and myeloarchitecture of the temporal lobe (Braak, 1980; Braak and Braak, 1985) and from his illustrations, one can observe the oblique wedge of dark signal in areas 35a and 35b that we observed in ex vivo MRI. The illustrations of Krimer and colleages also resemble, quite remarkably, the oblique pattern in area 35 (Krimer et al., 1997). Krimer's Gallyas staining appears so similar to our images that it is difficult to discern which is *ex vivo* MRI and which is Gallyas staining when viewed side by side. Insausti and colleagues (Insausti et al., 1995) also showed myelin staining in this region as well as Nissl staining where the oblique pattern in perirhinal cortex was observed in both stains, similarly noted in Braak's publications (Braak, 1980; Braak and Braak, 1985). The pattern in the Nissl stain, albeit more subtle in some cases, may require a neuroanatomically trained eye to appreciate. The *ex vivo* MRI contrast observed in perirhinal cortex, particularly in the oblique wedge, has a cyto-, pigmento-, and myeloarchitectural basis (Braak, 1980; Eickhoff et al., 2005; Krimer et al., 1997). Eickhoff and colleagues provided quantitative evidence for the concept that it was a mixture of contrast but that myelin contributed more than other properties to the observed MRI intensities (Eickhoff et al., 2005). Ex vivo validation will continue to play an important role in understanding MRI contrast and underlying myeloarchitecture in the human brain. The myeloarchitecture distribution and specificity of known pathways, bundles and cortical areas will validate *in vivo* studies and help to determine sequences and contrast that corroborate *ex vivo* findings with *in vivo* "myelin content", such as T1w/T2w ratio (Glasser and Van Essen, 2011), reciprocal of T1 (Sigalovsky et al., 2006) and decreased T2* in myelinated area (Cohen-Adad et al., 2012; van Gelderen et al., 2012) or increased T2* in demyelinated conditions (Lee et al., 2012).

The sulcal pattern in the MTL has also complicated the understanding of area 35 because the sulcal configurations vary considerably from human brain to human brain (Hanke, 1997; Insausti et al., 1995; Ono, 1990; Van Hoesen, 1995; Van Hoesen et al., 2000). The collateral sulcus is variable in length and depth, and at least 5 common patterns have been documented (non-interrupted, interrupted, interrupted but connected, interrupted and overlapped, multiple interruptions) (Bobinski et al., 1999; de Leon et al., 2004; Feczko et al., 2009; Goncharova et al., 2001; Hanke, 1997; Insausti et al., 1998; Insausti et al., 1995; Van Hoesen, 1995). The variability of the collateral sulcus together with similar, and arguably worse, variability in the incipient rhinal sulcus creates confusion for the identification of the underlying cortex that runs along both of these sulci, perirhinal cortex (area 35). It is important to emphasize that we labeled based on laminar features and not sulcal topography. Nonetheless, sulcal topography is worthy of discussion because so many studies define these two sulci and perirhinal incorrectly. Depending on the sulcal depth, perirhinal cortex can be larger than entorhinal cortex because it surrounds entorhinal on all sides, except for entorhinal's anterior border with primary olfactory cortex. Perirhinal cortex (area 35) spans two sulci (rhinal and collateral) and two gyri (anterior lateral temporal cortex and

parahippocampal). In this study, we define the rhinal sulcus as completely separate from the collateral sulcus (Braak and Braak, 1992; Ono, 1990; Suzuki and Amaral, 1994a; Van Hoesen, 1995; Van Hoesen et al., 2000) and do not ascribe to the rhinal sulcus being the anterior part of the collateral (Hanke, 1997). The sulcal boundaries for the entorhinal and perirhinal cortices can be elaborate, but in the most simple terms, a rhinal sulcus borders anteriorly and the collateral sulcus borders laterally. The entorhinal cortex lies medially, well within the boundaries of both sulci, on the crown of the anterior parahippocampal gyrus. The topography of perirhinal cortex is where the complexity is introduced because it resides in the depths of both sulci (rhinal and collateral) but on different banks in each. Perirhinal area 35 is positioned lateral to the rhinal sulcus but also medial to the collateral sulcus. Thus, perirhinal cortex is on the lateral bank of the rhinal sulcus and on the medial bank of the collateral sulcus. Perirhinal's location on the lateral bank of the rhinal sulcus in the human brain agrees with the position of the perirhinal cortex in non-human primates but the location on the medial bank of the collateral sulcus is unique to the human brain. The rhinal sulcus is absent in many human brains and is sometimes represented by a subtle groove or nothing at all, which is why it is often dubbed incipient. The collateral sulcus is more dependable and is routinely observed lateral to the entorhinal cortex and perirhinal area 35. Moreover, these complicated folding patterns such as the collateral and rhinal sulcus and intervening cortex, create problems for other registration or localization methods such as registration to a single template volume (i.e. Talairach volume), which may yield poor localization and poor accuracy because all common sulcal patterns were not represented. With *ex vivo* probabilistic mapping, multiple sulcal patterns are statistically summarized at multiple spatial scales and nearby sulci can help with localization of architectonics if the boundaries are consistent distances from stably occurring folds. This becomes important when research studies report that the right rhinal sulcus pattern was underrepresented in AD (Zhan et al., 2009), but given that the rhinal sulcus is extremely variable in humans and often it is so shallow that it is hardly a sulcus but instead a groove anteriorly, it is possible that the label was limited to the collateral sulcus. In contrast, the utilization of high resolution *ex vivo* labeling with the ability to assess cortical brain areas regardless of sulcal pattern, enables an accurate localization of perirhinal cortex. Cortical areas that occupy the depths of a sulcus and not the crown of a gyrus have not been well studied or localized due to previous technical limitations. The study of brain function depends on accurate and specific localization of anatomical areas, and lack of that - specificity and accuracy- can create a confounding factor in many studies. Our method and localization of perirhinal cortex provides a prototypical example of mapping areas that are hidden to an exterior observer (i.e. in sulcal depths).

Although this topic may seem like neuroanatomical minutiae, defining each area in the human brain becomes extremely important when diagnosing or predicting diagnoses or conversion to Alzheimer's disease, because these mesocortical areas in the MTL are the most vulnerable to NFT pathology in aging and AD. Area 35 and area 36 exhibit different pathological grades and at different times in the disease progression (Braak and Braak, 1991). Neurons in area 36 atrophy much later in the disease compared to area 35, which is the first area to display neurofibrillary tangles in aging and AD (Arnold et al., 1991b; Braak and Braak, 1991; Kemper, 1984; Knopman et al., 2003; Kordower et al., 2001; Van Hoesen et al., 2000). Others have used cortical thickness measures to illustrate more explicitly that the cortical ribbon is degenerating in these regions at an early stage (Dickerson et al., 2009a; Dickerson et al., 2009b; Dickerson et al., 2011) and likely reflects pathological cerebral atrophy. Our results showed differences between entorhinal and perirhinal cortical thickness in controls, MCI and AD patients and this method provides a more specific metric with area 35 alone than all medial temporal areas together. Furthermore, our tool allows mapping of perirhinal area 35 that has been validated with cortical architecture (i.e. histoarchitecture). Further analyses of cortical thickness were assessed and perirhinal exhibited the same

composition as entorhinal cortex with significant thinning in MCI and AD patients. Thus, MRI techniques have improved from a global atrophy measurement to now pinpointing specific areas, and this improvement may reflect and more accurately correlate with behavioral and cognitive scores in future studies.

Analogous to how anatomical definitions can confound disease-related analyses; functional consequences may be confounded as well. Animal and functional imaging studies have shown that perirhinal cortex detects novel objects, is required for object recognition, and forms an abstract representation of the object shown with delayed match and delayed non-match experiments, suggesting a role in memory (Barense et al., 2010; Brown and Aggleton, 2001; Buffalo et al., 2006; Murray et al., 2005; Murray and Mishkin, 1998). Thus, perirhinal cortex reveals activation when an object is novel and predicts familiarity-based recognition memory responses. Lesions of perirhinal in macaques have confirmed this novel detection of objects (Buckley and Gaffan, 1998; Murray and Mishkin, 1986; Suzuki et al., 1993; Zola-Morgan et al., 1989). A controversy exists regarding whether perirhinal cortex is involved in object recognition or object perception (Hampton, 2005; Murray et al., 2000). Imprecise anatomical definitions or grouping multiple areas are commonly proliferated in functional imaging studies. Devlin et al argue that perirhinal cortex is involved in visual perception and also in memory and language (Devlin and Price, 2007). This raises the question: is this the case because humans rely mainly on visual input, or is it because the anatomical area defined was large (area 35 + area 36) and included a substantial visual associative area (isocortical area 36)? Cognitive neurobiologists have noted the controversy where Hampton outlined the problems that arose from methodological distinctions regarding perception and memory (Buckley and Gaffan, 1998; Hampton, 2005). Perhaps careful fMRI studies that explicitly define perirhinal as area 35 only can distinguish more specific function for perirhinal and distinguish it from surrounding cortices. Our probabilistic mapping provides an accurate localization of perirhinal cortex and may help future application studies define area 35, and further characterize its functional properties. Functional MRI, behavioral or cognitive studies are predicated on accurate anatomical localization and when a precise localization does not occur, results can be confounded and difficult to interpret.

Conclusion

Understanding cortical areas that traverse more than one gyrus or sulcus is an important task and critical in assessment of normal brain function as well as disease states. Several imaging studies have utilized a volumetric approach to evaluate and predict the state of atrophy in the MTL in AD. As quantitative measures evolve in imaging from global atrophy to specific metrics such as cortical thickness, it is important to accurately assess each anatomical area in healthy controls, non-demented aging and AD, as well as other neurodegenerative disorders. Our *ex vivo* probabilistic mapping of perirhinal cortex provides significant benefits in this endeavor in the form of specific, histologically validated, automated and accurate labeling of architectonic regions in the MTL, facilitating the analysis of atrophic change in a large dataset for earlier detection and diagnosis of the many diseases that affect the MTL. Refined detection of individual areas will enable accurate localization and assessment of smaller, more homogeneously affected brain areas, facilitating earlier detection of disease processes, and enhancing the possibility of therapeutic intervention before widespread cell death.

Acknowledgments

We would like to thank those who donated tissue; their generous donation made this work possible. We extend special thanks to Brad Dickerson for reading this manuscript and helpful comments. Support for this research was provided in part by the National Center for Research Resources (P41-RR14075, and the NCRR BIRN Morphometric Project BIRN002, U24 RR021382), the National Institute for Biomedical Imaging and Bioengineering (R01EB006758), the National Institute on Aging (AG022381) and (AG028521), the Massachusetts (MGH) Alzheimer's Disease Resource Center (5P50AG005134-28), Boston University Alzheimer's Disease Center

and Framingham Heart Study (P30-AG13846 and R01 AG1649), the National Center for Alternative Medicine (RC1AT005728-01), the National Institute for Neurological Disorders and Stroke (R01 NS052585-01, 1R21NS072652-01, 1R01NS070963), and was made possible by the resources provided by Shared Instrumentation Grants 1S10RR023401, 1S10RR019307, and 1S10RR023043. Additional support was provided by The Autism & Dyslexia Project funded by the Ellison Medical Foundation and by the NIH Blueprint for Neuro-science Research (U01-MH093765, part of the multi-institutional Human Connectome Project). Data collection and sharing for this project was funded by the Alzheimer's Disease Neuroimaging Initiative (ADNI) (National Institutes of Health Grant U01 AG024904). ADNI is funded by the National Institute on Aging, the National Institute of Biomedical Imaging and Bioengineering, and through generous contributions from the following: Abbott; Alzheimer's Association; Alzheimer's Drug Discovery Foundation; Amorfix Life Sciences Ltd.; AstraZeneca; Bayer HealthCare; BioClinica, Inc.; Biogen Idec Inc.; Bristol-Myers Squibb Company; Eisai Inc.; Elan Pharmaceuticals Inc.; Eli Lilly and Company; F. Hoffmann-La Roche Ltd and its affiliated company Genentech, Inc.; GE Healthcare; Innogenetics, N.V.; Janssen Alzheimer Immunotherapy Research & Development, LLC.; Johnson & Johnson Pharmaceutical Research & Development LLC.; Medpace, Inc.; Merck & Co., Inc.; Meso Scale Diagnostics, LLC.; Novartis Pharmaceuticals Corporation; Pfizer Inc.; Servier; Synarc Inc.; and Takeda Pharmaceutical Company. The Canadian Institutes of Health Research is providing funds to support ADNI clinical sites in Canada. Private sector contributions are facilitated by the Foundation for the National Institutes of Health (www.fnih.org). The grantee organization is the Northern California Institute for Research and Education, and the study is coordinated by the Alzheimer's Disease Cooperative Study at the University of California, San Diego. ADNI data are disseminated by the Laboratory for Neuro Imaging at the University of California, Los Angeles. This research was also supported by NIH grants P30 AG010129, K01 AG030514, and the Dana Foundation.

References

Arnold SE, Hyman BT, Flory J, Damasio AR, Van Hoesen GW. The topographical and neuroanatomical distribution of neurofibrillary tangles and neuritic plaques in the cerebral cortex of patients with Alzheimer's disease. Cereb Cortex. 1991a; 1:103–116. [PubMed: 1822725]

Arnold SE, Hyman BT, Van Hoesen GW, Damasio AR. Some cytoarchitectural abnormalities of the entorhinal cortex in schizophrenia. Arch Gen Psychiatry. 1991b; 48:625–632. [PubMed: 2069493]

Augustinack JC, Helmer K, Huber KE, Kakunoori S, Zollei L, Fischl B. Direct visualization of the perforant pathway in the human brain with ex vivo diffusion tensor imaging. Front Hum Neurosci. 2010; 4:42. [PubMed: 20577631]

Augustinack JC, van der Kouwe AJ, Blackwell ML, Salat DH, Wiggins CJ, Frosch MP, Wiggins GC, Potthast A, Wald LL, Fischl BR. Detection of entorhinal layer II using 7Tesla magnetic resonance imaging. Ann Neurol. 2005; 57:489–494. [PubMed: 15786476]

Barense MD, Henson RN, Lee AC, Graham KS. Medial temporal lobe activity during complex discrimination of faces, objects, and scenes: Effects of viewpoint. Hippocampus. 2010; 20:389–401. [PubMed: 19499575]

Bobinski M, de Leon MJ, Convit A, De Santi S, Wegiel J, Tarshish CY, Saint Louis LA, Wisniewski HM. MRI of entorhinal cortex in mild Alzheimer's disease. Lancet. 1999; 353:38–40. [PubMed: 10023955]

Bock NA, Kocharyan A, Liu JV, Silva AC. Visualizing the entire cortical myelination pattern in marmosets with magnetic resonance imaging. J Neurosci Methods. 2009; 185:15–22. [PubMed: 19737577]

Braak, H. Studies of Brain Function. Springer-Verlag; Berlin Heidleberg: 1980. Architectonics of the Human Telencephalic Cortex; p. 42-48.

Braak H, Braak E. On areas of transition between entorhinal allocortex and temporal isocortex in the human brain. Normal morphology and lamina-specific pathology in Alzheimer's disease. Acta Neuropathol. 1985; 68:325–332. [PubMed: 4090943]

Braak H, Braak E. Neuropathological stageing of Alzheimer-related changes. Acta Neuropathol (Berl). 1991; 82:239–259. [PubMed: 1759558]

Braak H, Braak E. The human entorhinal cortex: normal morphology and lamina-specific pathology in various diseases. Neurosci Res. 1992; 15:6–31. [PubMed: 1336586]

Brodmann, K. Vergleichende Lokalisationslehre der Groshirnrinde. Verlag von Johann Ambrosius Barth; Leipzig: 1909.

Brodmann, K.; Garey, L. Brodmann's Localisation in the Cerebral Cortex. Smith-Gordon; London: 1994.

Brown MW, Aggleton JP. Recognition memory: what are the roles of the perirhinal cortex and hippocampus? Nat Rev Neurosci. 2001; 2:51–61. [PubMed: 11253359]

Buckley MJ, Gaffan D. Perirhinal cortex ablation impairs visual object identification. J Neurosci. 1998; 18:2268–2275. [PubMed: 9482811]

Buffalo EA, Bellgowan PS, Martin A. Distinct roles for medial temporal lobe structures in memory for objects and their locations. Learn Mem. 2006; 13:638–643. [PubMed: 16980544]

Cohen-Adad J, Polimeni JR, Helmer KG, Benner T, McNab JA, Wald LL, Rosen BR, Mainero C. T(2)* mapping and B(0) orientation-dependence at 7 T reveal cyto- and myeloarchitecture organization of the human cortex. Neuroimage. 2012; 60:1006–1014. [PubMed: 22270354]

Dale AM, Fischl B, Sereno MI. Cortical surface-based analysis. I. Segmentation and surface reconstruction. Neuroimage. 1999; 9:179–194. [PubMed: 9931268]

de Leon MJ, DeSanti S, Zinkowski R, Mehta PD, Pratico D, Segal S, Clark C, Kerkman D, DeBernardis J, Li J, Lair L, Reisberg B, Tsui W, Rusinek H. MRI and CSF studies in the early diagnosis of Alzheimer's disease. J Intern Med. 2004; 256:205–223. [PubMed: 15324364]

De Toledo-Morrell L, Goncharova I, Dickerson B, Wilson RS, Bennett DA. From healthy aging to early Alzheimer's disease: in vivo detection of entorhinal cortex atrophy. Ann N Y Acad Sci. 2000; 911:240–253. [PubMed: 10911878]

Devlin JT, Price CJ. Perirhinal contributions to human visual perception. Curr Biol. 2007; 17:1484–1488. [PubMed: 17764947]

Dickerson BC, Bakkour A, Salat DH, Feczko E, Pacheco J, Greve DN, Grodstein F, Wright CI, Blacker D, Rosas HD, Sperling RA, Atri A, Growdon JH, Hyman BT, Morris JC, Fischl B, Buckner RL. The cortical signature of Alzheimer's disease: regionally specific cortical thinning relates to symptom severity in very mild to mild AD dementia and is detectable in asymptomatic amyloid-positive individuals. Cereb Cortex. 2009a; 19:497–510. [PubMed: 18632739]

Dickerson BC, Feczko E, Augustinack JC, Pacheco J, Morris JC, Fischl B, Buckner RL. Differential effects of aging and Alzheimer's disease on medial temporal lobe cortical thickness and surface area. Neurobiol Aging. 2009b; 30:432–440. [PubMed: 17869384]

Dickerson BC, Stoub TR, Shah RC, Sperling RA, Killiany RJ, Albert MS, Hyman BT, Blacker D, Detoledo-Morrell L. Alzheimer-signature MRI biomarker predicts AD dementia in cognitively normal adults. Neurology. 2011; 76:1395–1402. [PubMed: 21490323]

Ding SL, Van Hoesen GW. Borders, extent, and topography of human perirhinal cortex as revealed using multiple modern neuroanatomical and pathological markers. Hum Brain Mapp. 2010; 31:1359–1379. [PubMed: 20082329]

Ding SL, Van Hoesen GW, Cassell MD, Poremba A. Parcellation of human temporal polar cortex: a combined analysis of multiple cytoarchitectonic, chemoarchitectonic, and pathological markers. J Comp Neurol. 2009; 514:595–623. [PubMed: 19363802]

Duyn JH, van Gelderen P, Li TQ, de Zwart JA, Koretsky AP, Fukunaga M. High-field MRI of brain cortical substructure based on signal phase. Proc Natl Acad Sci U S A. 2007; 104:11796–11801. [PubMed: 17586684]

Eickhoff S, Walters NB, Schleicher A, Kril J, Egan GF, Zilles K, Watson JD, Amunts K. High-resolution MRI reflects myeloarchitecture and cytoarchitecture of human cerebral cortex. Hum Brain Mapp. 2005; 24:206–215. [PubMed: 15543596]

Feczko E, Augustinack JC, Fischl B, Dickerson BC. An MRI-based method for measuring volume, thickness and surface area of entorhinal, perirhinal, and posterior parahippocampal cortex. Neurobiol Aging. 2009; 30:420–431. [PubMed: 17850926]

Fischl B, Liu A, Dale AM. Automated manifold surgery: constructing geometrically accurate and topologically correct models of the human cerebral cortex. IEEE Trans Med Imaging. 2001; 20:70–80. [PubMed: 11293693]

Fischl B, Sereno MI, Dale AM. Cortical surface-based analysis. II: Inflation, flattening, and a surface-based coordinate system. Neuroimage. 1999a; 9:195–207. [PubMed: 9931269]

Fischl B, Sereno MI, Tootell RB, Dale AM. High-resolution intersubject averaging and a coordinate system for the cortical surface. Hum Brain Mapp. 1999b; 8:272–284. [PubMed: 10619420]

Fischl B, Stevens AA, Rajendran N, Yeo BT, Greve DN, Van Leemput K, Polimeni JR, Kakunoori S, Buckner RL, Pacheco J, Salat DH, Melcher J, Frosch MP, Hyman BT, Grant PE, Rosen BR, van

der Kouwe AJ, Wiggins GC, Wald LL, Augustinack JC. Predicting the location of entorhinal cortex from MRI. Neuroimage. 2009; 47:8–17. [PubMed: 19376238]

Fukunaga M, Li TQ, van Gelderen P, de Zwart JA, Shmueli K, Yao B, Lee J, Maric D, Aronova MA, Zhang G, Leapman RD, Schenck JF, Merkle H, Duyn JH. Layer-specific variation of iron content in cerebral cortex as a source of MRI contrast. Proc Natl Acad Sci USA. 2010; 107:3834–3839. [PubMed: 20133720]

Geyer S, Weiss M, Reimann K, Lohmann G, Turner R. Microstructural Parcellation of the Human Cerebral Cortex - From Brodmann's Post-Mortem Map to in vivo Mapping with High-Field Magnetic Resonance Imaging. Front Hum Neurosci. 2011; 5:19. [PubMed: 21373360]

Glasser MF, Van Essen DC. Mapping human cortical areas in vivo based on myelin content as revealed by T1- and T2-weighted MRI. J Neurosci. 2011; 31:11597–11616. [PubMed: 21832190]

Gloor, P. The Temporal Lobe and Limbic System. Oxford University Press; New York, New York: 1997.

Goncharova, Dickerson BC, Stoub TR, deToledo-Morrell L. MRI of human entorhinal cortex: a reliable protocol for volumetric measurement. Neurobiol Aging. 2001; 22:737–745. [PubMed: 11705633]

Hampton RR. Monkey perirhinal cortex is critical for visual memory, but not for visual perception: reexamination of the behavioural evidence from monkeys. Q J Exp Psychol B. 2005; 58:283–299. [PubMed: 16194970]

Hanke J. Sulcal pattern of the anterior parahippocampal gyrus in the human adult. Ann Anat. 1997; 179:335–339. [PubMed: 9272217]

Insausti R, Juottonen K, Soininen H, Insausti AM, Partanen K, Vainio P, Laakso MP, Pitkanen A. MR volumetric analysis of the human entorhinal, perirhinal, and temporopolar cortices. AJNR Am J Neuroradiol. 1998; 19:659–671. [PubMed: 9576651]

Insausti R, Tunon T, Sobreviela T, Insausti AM, Gonzalo LM. The human entorhinal cortex: a cytoarchitectonic analysis. J Comp Neurol. 1995; 355:171–198. [PubMed: 7541808]

Jack CR Jr. Bernstein MA, Fox NC, Thompson P, Alexander G, Harvey D, Borowski B, Britson PJ, J LW, Ward C, Dale AM, Felmlee JP, Gunter JL, Hill DL, Killiany R, Schuff N, Fox-Bosetti S, Lin C, Studholme C, DeCarli CS, Krueger G, Ward HA, Metzger GJ, Scott KT, Mallozzi R, Blezek D, Levy J, Debbins JP, Fleisher AS, Albert M, Green R, Bartzokis G, Glover G, Mugler J, Weiner MW. The Alzheimer's Disease Neuroimaging Initiative (ADNI): MRI methods. J Magn Reson Imaging. 2008; 27:685–691. [PubMed: 18302232]

Jack CR Jr. Petersen RC, Xu YC, Waring SC, O'Brien PC, Tangalos EG, Smith GE, Ivnik RJ, Kokmen E. Medial temporal atrophy on MRI in normal aging and very mild Alzheimer's disease. Neurology. 1997; 49:786–794. [PubMed: 9305341]

Kaye JA, Swihart T, Howieson D, Dame A, Moore MM, Karnos T, Camicioli R, Ball M, Oken B, Sexton G. Volume loss of the hippocampus and temporal lobe in healthy elderly persons destined to develop dementia. Neurology. 1997; 48:1297–1304. [PubMed: 9153461]

Kemper, T. Neuroanatomical and neuropathological changes in normal aging and in dementia. In: Albert, ML.; Knopefel, JE., editors. Clinical Neurology of Aging. Oxford Univerisity Press; New York, NY: 1984. p. 9-52.

Killiany RJ, Gomez-Isla T, Moss M, Kikinis R, Sandor T, Jolesz F, Tanzi R, Jones K, Hyman BT, Albert MS. Use of structural magnetic resonance imaging to predict who will get Alzheimer's disease. Ann Neurol. 2000; 47:430–439. [PubMed: 10762153]

Killiany RJ, Hyman BT, Gomez-Isla T, Moss MB, Kikinis R, Jolesz F, Tanzi R, Jones K, Albert MS. MRI measures of entorhinal cortex vs hippocampus in preclinical AD. Neurology. 2002; 58:1188–1196. [PubMed: 11971085]

Knopman DS, Parisi JE, Salviati A, Floriach-Robert M, Boeve BF, Ivnik RJ, Smith GE, Dickson DW, Johnson KA, Petersen LE, McDonald WC, Braak H, Petersen RC. Neuropathology of cognitively normal elderly. J Neuropathol Exp Neurol. 2003; 62:1087–1095. [PubMed: 14656067]

Kordower JH, Chu Y, Stebbins GT, DeKosky ST, Cochran EJ, Bennett D, Mufson EJ. Loss and atrophy of layer II entorhinal cortex neurons in elderly people with mild cognitive impairment. Ann Neurol. 2001; 49:202–213. [PubMed: 11220740]

Krimer LS, Hyde TM, Herman MM, Saunders RC. The entorhinal cortex: an examination of cyto- and myeloarchitectonic organization in humans. Cereb Cortex. 1997; 7:722–731. [PubMed: 9408036]

Langkammer C, Krebs N, Goessler W, Scheurer E, Yen K, Fazekas F, Ropele S. Susceptibility induced gray-white matter MRI contrast in the human brain. Neuroimage. 2012; 59:1413–1419. [PubMed: 21893208]

Lee J, Shmueli K, Kang BT, Yao B, Fukunaga M, van Gelderen P, Palumbo S, Bosetti F, Silva AC, Duyn JH. The contribution of myelin to magnetic susceptibility-weighted contrasts in high-field MRI of the brain. Neuroimage. 2012; 59:3967–3975. [PubMed: 22056461]

Mesulam, MM.; Mufson, EJ. The Insula of Reil in Man and Monkey. In: Peters, A.; Jones, EG., editors. Cerebral Cortex, Association and Auditory Cortices. Plenum Press; New York: 1985. p. 179-226.

Meunier M, Bachevalier J, Mishkin M, Murray EA. Effects on visual recognition of combined and separate ablations of the entorhinal and perirhinal cortex in rhesus monkeys. J Neurosci. 1993; 13:5418–5432. [PubMed: 8254384]

Meunier M, Hadfield W, Bachevalier J, Murray EA. Effects of rhinal cortex lesions combined with hippocampectomy on visual recognition memory in rhesus monkeys. J Neurophysiol. 1996; 75:1190–1205. [PubMed: 8867128]

Mugler JP 3rd, Brookeman JR. Rapid three-dimensional T1-weighted MR imaging with the MP-RAGE sequence. J Magn Reson Imaging. 1991; 1:561–567. [PubMed: 1790381]

Murray EA, Bussey TJ, Hampton RR, Saksida LM. The parahippocampal region and object identification. Ann N Y Acad Sci. 2000; 911:166–174. [PubMed: 10911873]

Murray EA, Graham KS, Gaffan D. Perirhinal cortex and its neighbours in the medial temporal lobe: contributions to memory and perception. Q J Exp Psychol B. 2005; 58:378–396. [PubMed: 16194975]

Murray EA, Mishkin M. Visual recognition in monkeys following rhinal cortical ablations combined with either amygdalectomy or hippocampectomy. J Neurosci. 1986; 6:1991–2003. [PubMed: 3734871]

Murray EA, Mishkin M. Object recognition and location memory in monkeys with excitotoxic lesions of the amygdala and hippocampus. J Neurosci. 1998; 18:6568–6582. [PubMed: 9698344]

Ono, M.; Kubik, S.; Abernathey, CD. Atlas of the Cerebral Sulci. Georg Thieme Verlag; New York: 1990.

Pandya, DN.; Yeterian, E. Architecture and Connections of Cortical Association Areas. In: Peters, A.; Jones, EG., editors. Cerebral Cortex, Association and Auditory Cortices. Plenum Press; New York: 1985. p. 179-226.

Petersen RC, Aisen PS, Beckett LA, Donohue MC, Gamst AC, Harvey DJ, Jack CR Jr. Jagust WJ, Shaw LM, Toga AW, Trojanowski JQ, Weiner MW. Alzheimer's Disease Neuroimaging Initiative (ADNI): clinical characterization. Neurology. 2010; 74:201–209. [PubMed: 20042704]

Rosene, DL.; Van Hoesen, GW. Cerebral Cortex. In: Jones, EG.; Peters, A., editors. Cerebral Cortex, Further Aspects of Cortical Function, Including Hippocampus. Plenum Press; New York, New York: 1987.

Sanides F. Comparative architectonics of the neocortex of mammals and their evolutionary interpretation. Annals of the New York Academy of Sciences. 1969; 167:404–423.

Sanides, F. Functional architecture of motor and sensory cortices in primates in light of a new concept of neocortical evolution. In: Noback, CR.; Montagna, W., editors. The Primate Brain, Advances in Primatology. Appleton-Century Crofts; New York: 1970. p. 137-208.

Segonne F, Dale AM, Busa E, Glessner M, Salat D, Hahn HK, Fischl B. A hybrid approach to the skull stripping problem in MRI. Neuroimage. 2004; 22:1060–1075. [PubMed: 15219578]

Sigalovsky IS, Fischl B, Melcher JR. Mapping an intrinsic MR property of gray matter in auditory cortex of living humans: a possible marker for primary cortex and hemispheric differences. Neuroimage. 2006; 32:1524–1537. [PubMed: 16806989]

Solodkin A, Van Hoesen GW. Entorhinal cortex modules of the human brain. J Comp Neurol. 1996; 365:610–617. [PubMed: 8742306]

Stephan, H. In Handbuch der mikroskopischen Anatomie des Menschen. Springer-Verlag; Berlin and New York: 1975.

Suzuki WA, Amaral DG. Perirhinal and parahippocampal cortices of the macaque monkey: cortical afferents. J Comp Neurol. 1994a; 350:497–533. [PubMed: 7890828]

Suzuki WA, Amaral DG. Topographic organization of the reciprocal connections between the monkey entorhinal cortex and the perirhinal and parahippocampal cortices. J Neurosci. 1994b; 14:1856–1877. [PubMed: 8126576]

Suzuki WA, Amaral DG. Perirhinal and parahippocampal cortices of the macaque monkey: cytoarchitectonic and chemoarchitectonic organization. J Comp Neurol. 2003a; 463:67–91. [PubMed: 12811804]

Suzuki WA, Amaral DG. Where are the perirhinal and parahippocampal cortices? A historical overview of the nomenclature and boundaries applied to the primate medial temporal lobe. Neuroscience. 2003b; 120:893–906. [PubMed: 12927196]

Suzuki WA, Zola-Morgan S, Squire LR, Amaral DG. Lesions of the perirhinal and parahippocampal cortices in the monkey produce long-lasting memory impairment in the visual and tactual modalities. J Neurosci. 1993; 13:2430–2451. [PubMed: 8501516]

Taylor KI, Probst A. Anatomic localization of the transentorhinal region of the perirhinal cortex. Neurobiol Aging. 2008; 29:1591–1596. [PubMed: 17478012]

van Gelderen P, de Zwart JA, Lee J, Sati P, Reich DS, Duyn JH. Nonexponential T(2) decay in white matter. Magn Reson Med. 2012; 67:110–117. [PubMed: 21630352]

Van Hoesen G, Pandya DN. Some connections of the entorhinal (area 28) and perirhinal (area 35) cortices of the rhesus monkey. I. Temporal lobe afferents. Brain Res. 1975a; 95:1–24. [PubMed: 1156859]

Van Hoesen GW. Anatomy of the medial temporal lobe. Magn Reson Imaging. 1995; 13:1047–1055. [PubMed: 8750316]

Van Hoesen GW, Augustinack JC, Dierking J, Redman SJ, Thangavel R. The parahippocampal gyrus in Alzheimer's disease. Clinical and preclinical neuroanatomical correlates. Ann N Y Acad Sci. 2000; 911:254–274. [PubMed: 10911879]

Van Hoesen GW, Pandya DN. Some connections of the entorhinal (area 28) and perirhinal (area 35) cortices of the rhesus monkey. III. Efferent connections. Brain Res. 1975b; 95:39–59. [PubMed: 1156868]

Van Hoesen GW, Solodkin A. Some modular features of temporal cortex in humans as revealed by pathological changes in Alzheimer's disease. Cereb Cortex. 1993; 3:465–475. [PubMed: 7505138]

von Economo, CF.; Koskinas, GN. Die Cytoarchitektonik der Hirnrinde des erwachsenen Menschen (Cytoarchitectonics of the Adult Human Cerebral Cortex). Springer; Berlin: 1925.

Xu Y, Jack CR Jr. O'Brien PC, Kokmen E, Smith GE, Ivnik RJ, Boeve BF, Tangalos RG, Petersen RC. Usefulness of MRI measures of entorhinal cortex versus hippocampus in AD. Neurology. 2000; 54:1760–1767. [PubMed: 10802781]

Zhan J, Brys M, Glodzik L, Tsui W, Javier E, Wegiel J, Kuchna I, Pirraglia E, Li Y, Mosconi L, Saint Louis LA, Switalski R, De Santi S, Kim BC, Wisniewski T, Reisberg B, Bobinski M, de Leon MJ. An entorhinal cortex sulcal pattern is associated with Alzheimer's disease. Hum Brain Mapp. 2009; 30:874–882. [PubMed: 18381771]

Zola-Morgan S, Squire LR, Amaral DG, Suzuki WA. Lesions of perirhinal and parahippocampal cortex that spare the amygdala and hippocampal formation produce severe memory impairment. J Neurosci. 1989; 9:4355–4370. [PubMed: 2593004]

Highlights

- Localized human perirhinal cortex using *ex vivo* MRI volumes.
- Validated localization of perirhinal cortex with cytoarchitectural Nissl staining.
- Mapped perirhinal labels from high resolution *ex vivo* to flattened spherical space.
- Hausdorff distance measures were compared for right and left hemispheres.
- Cortical thickness showed differences between controls and Alzheimer's disease.

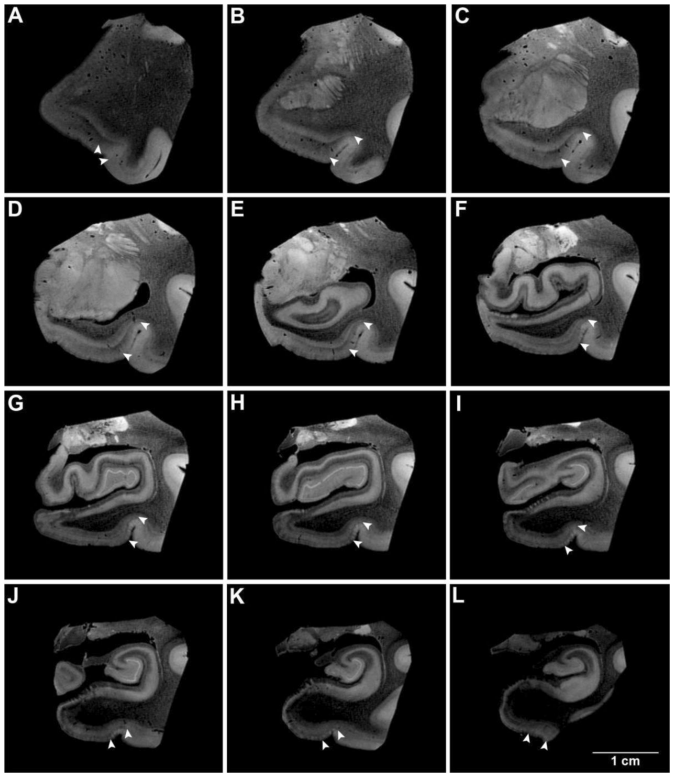

Figure 1.
Anterior-posterior coronal slices that demonstrate perirhinal cortex in *ex vivo* MRI. Several *ex vivo* MRI slices demonstrate detection of perirhinal cortex (area 35) throughout its rostrocaudal extent in one selected case (67 year old, male). Note the vertical columnar structures in 35a and the oblique wedge in entire area 35 that indicate perirhinal cortex. White carets represent the medial and lateral borders in panels A–L.

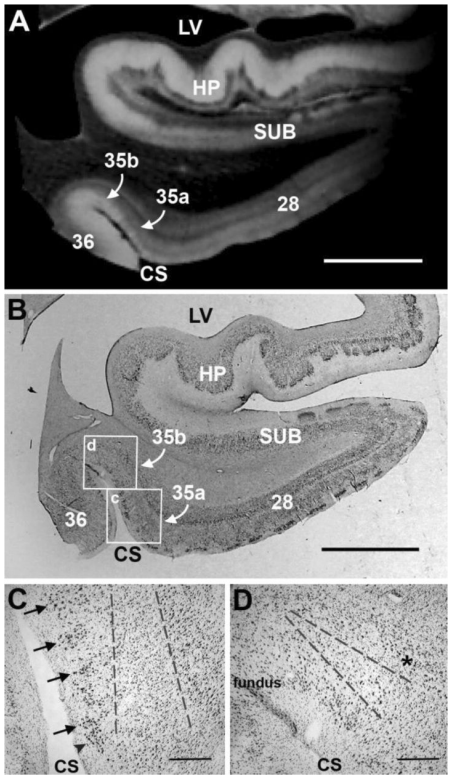

Figure 2.

Histological validation of perirhinal cortex in *ex vivo* MRI. High resolution FLASH image (100 μm isotropic) that reveals columnar contrast in area 35a medially and lighter contrast superficially and laterally in area 35b in (A). The corresponding histological slice is illustrated in (B) with boxed insets for higher magnification photos of area 35a and area 35b respectively in (C) and (D). Black arrows point to the columns in perirhinal 35a and dotted lines in infragranular lamina represent the medial portion of the oblique wedge observed in *ex vivo* MRI in (C). With the collateral sulcus fundus on the left, (D) shows the histological slice of area 35b and the lateral portion of the oblique wedge. The asterisk (*) denotes layer V in area 35b. Magnification bar = 5 mm in (A) and (B). Magnification bar = 500 μm in (C) and (D).

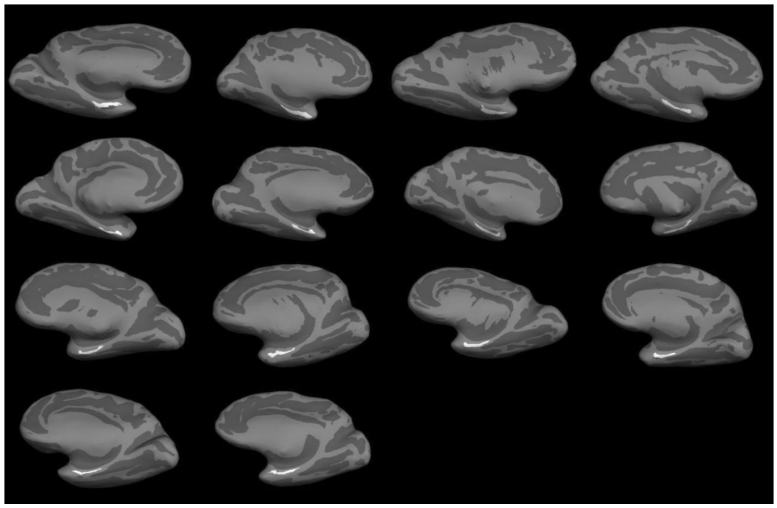

Figure 3.
Fourteen cases were labeled on high resolution *ex vivo* MRI volumes and mapped to respective individual surface maps. Each inflated brain shows the location of perirhinal cortex (area 35) for each case labeled in white.

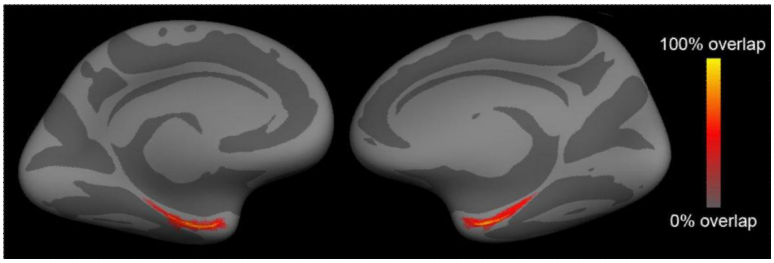

Figure 4.

Average probabilistic maps for perirhinal cortex. Each case label was mapped onto an existing template - fsaverage - where labels overlapped to show high probability of localization in this ventromedial view. Yellow represents 100% overlap among cases.

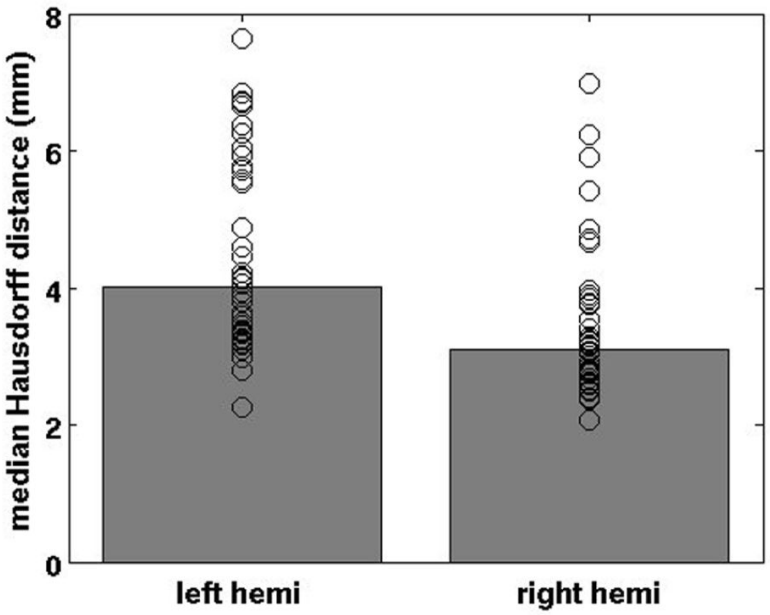

Figure 5.
Median Hausdorff distance in perirhinal cortex. The Hausdorff distance was computed from the manual labels and the mapped label. The mean distance was 4.0 mm for left hemisphere and 3.2 mm for the right hemisphere and the Hausdorff distance was slightly more variable in left than right hemispheres.

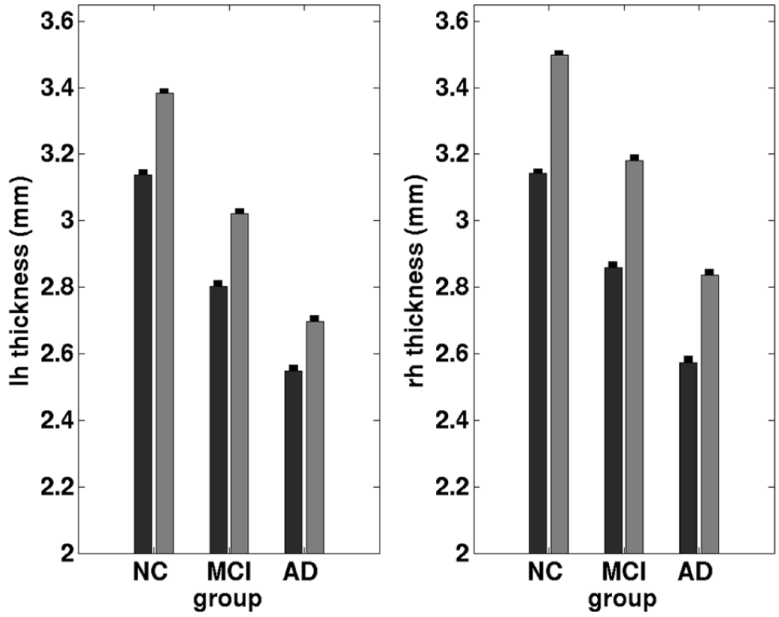

Figure 6.

Cortical thickness measures for ADNI subjects in left and right hemispheres in controls, mild cognitive impairment and Alzheimer's disease. The black bars represent perirhinal cortex (area 35) and the gray bars represent entorhinal cortex (area 28). Note the perirhinal cortex is thinner than the entorhinal cortex in each group but shows the same pattern of atrophy as entorhinal cortex. Error bars represent standard error of the mean for each group.